Interaction of Tropical Deep Convection with the Large-Scale Circulation in the MJO

ERIC TROMEUR AND WILLIAM B. ROSSOW

National Oceanic and Atmospheric Administration/Cooperative Remote Sensing of Science and Technology Center, The City College of New York, New York, New York

(Manuscript received 12 May 2009, in final form 24 September 2009)

ABSTRACT

To better understand the interaction between tropical deep convection and the Madden–Julian oscillation (MJO), tropical cloud regimes are defined by cluster analysis of International Satellite Cloud Climatology Project (ISCCP) cloud-top pressure—optical thickness joint distributions from the D1 dataset covering 21.5 yr. An MJO index based solely on upper-level wind anomalies is used to study variations of the tropical cloud regimes. The MJO index shows that MJO events are present almost all the time; instead of the MJO event being associated with ''on or off'' deep convection, it is associated with weaker or stronger mesoscale organization of deep convection. Atmospheric winds and humidity from NCEP–NCAR reanalysis 1 are used to characterize the large-scale dynamics of the MJO; the results show that the large-scale motions initiate an MJO event by moistening the lower troposphere by horizontal advection. Increasingly strong convection transports moisture into the upper troposphere, suggesting a reinforcement of the convection itself. The change of convection organization shown by the cloud regimes indicates a strong interaction between the large-scale circulation and deep convection. The analysis is extended to the complete atmospheric diabatic heating by precipitation, radiation, and surface fluxes. The wave organizes stronger convective heating of the tropical atmosphere, which results in stronger winds, while there is only a passive response of the surface, directly linked to cloud radiative effects. Overall, the results suggest that an MJO event is an amplification of large-scale wave motions by stronger convective heating, which results from a dynamic reorganization of scattered deep convection into more intense mesoscale systems.

1. Introduction

The Madden–Julian oscillation (MJO) is a fundamental mode of tropical low-frequency variability (Madden and Julian 1994) that usually appears first over the Indian Ocean and is characterized by an eastward propagation of a region of enhanced tropical deep convection and rainfall into the western Pacific with a time scale of 30–60 days. Intra-annual variations of the MJO affect the intensity and the break periods of the Indian and Asian–Australian monsoons (Hendon and Liebmann 1990). Recent studies also suggest a possible role of the MJO in El Niño–Southern Oscillation (ENSO) (Slingo et al. 1999), the lifetime of the MJO being dependent on the state of ENSO (Pohl and Matthews 2007).

A number of theories have been proposed to explain the MJO (Majda et al. 2007) such as evaporation–wind feedback, also known as wind-induced surface heat exchange (WISHE) (Emanuel 1987; Neelin et al. 1987), boundary layer frictional convective convergence (Wang and Rui 1990; Maloney and Hartmann 1998), stochastic linearized convection (Salby et al. 1994), radiation instability (Raymond 2001), planetary-scale linear response to moving heat sources (Chao 1987), extratropical wave forcing organizing the convection (Bladé and Hartmann 1993), and the wave-convective instability of the second kind (CISK) theory (Bladé and Hartmann 1993; Chao and Chen 2001). Moncrieff (2004) recently developed a nonlinear theory for the upscale transport of momentum from equatorial mesoscales to planetary scales and used this theory to explain the ''MJO-like'' structure in recent ''superparameterization'' model simulations with a scale gap between 200 and 1200 km.

Despite the many studies published in the past 30 years, we still do not have a clear understanding of the MJO [Raymond (2001) calls this the Holy Grail of

Corresponding author address: Dr. Eric Tromeur, NOAA/CREST Center, Remote Sensing of Climate Group, The City College of New York, Steinman Hall (T-107), New York, NY 10031.
E-mail: etromeur@ccny.cuny.edu

DOI: 10.1175/2009JCLI3240.1

tropical atmospheric dynamics]. There are three most popular theories. The first (Maloney and Hartmann 1998) proposes that frictional convergence in front of propagating convection slowly moistens the atmosphere to a state that is more favorable for convection. Such a moistening provides a mechanism for slow eastward propagation but does not explain where the (presumably) enhanced convection comes from to begin with or why the MJO is only occasionally present in boreal winter and only in the Indo-Pacific region. The second (wave-CISK theory) proposes that the interaction between equatorial waves and cumulus convection is unstable so that it produces mixed Rossby–Kelvin waves but does not explain the source of the initiating waves. The third assumes that extratropical wave forcing organizes the convection but further development is associated with the wave-CISK theory.

Recent studies focus on GCM simulations of the MJO (Mu and Zhang 2008; Slingo et al. 1996), but these are still problematic (Zhang 2005). The poor model representation of the MJO and lack of success in developing a theory of it that predicts its general characteristics suggest that the theories and models lack something vital that maintains the oscillation. One question is the precise link between the nature of tropical convection and large-scale tropical waves. Which comes first—if that is a meaningful question? Do the waves organize and amplify convection that is already present or does convection create and amplify the waves? Is the interaction primarily about energy or momentum exchanges? Notice that these questions are posed in terms of only two dynamic components, large-scale waves and convection, as if there is only one of each. So an additional question is whether there are more interacting components involved.

The goal of this study is to investigate the observed convection characteristics and energy exchanges in an interaction with large-scale atmospheric motions to evaluate the theories of the MJO. For this purpose, tropical cloud regimes are defined by cluster analysis of International Satellite Cloud Climatology Project (ISCCP) cloud-top pressure (CTP)–optical thickness (τ) joint distributions from the ISCCP D1 dataset (Rossow and Schiffer 1999). This cluster analysis approach allows us to identify distinct weather states related to different tropical cloud regimes as in Jakob and Tselioudis (2003) and Rossow et al. (2005). These regimes are then used to characterize organized and disorganized convection as a function of MJO phase, using an MJO index. Finally, composites of data products quantifying precipitation, atmospheric radiative heating, ocean surface energy fluxes, and the large-scale atmospheric state and motions are examined to elucidate the nature and timing of convection–wave energy exchanges.

The clustering method used to define the cloud regimes is described in section 2 before introducing the MJO index. The choice of the index threshold to characterize an MJO event is not obvious and is further investigated. In section 3, the variation of the tropical cloud regimes with the MJO phase are shown as composite relative frequency of occurrence (RFO) for each cloud regimes (weather state). Composite vertical and horizontal velocities, as well as specific humidity, are also analyzed in order to explore the interaction between tropical convection and the large-scale circulation in the MJO. In particular, we want to evaluate the quality of reanalysis data and to make sure that weak MJOs observed in our analysis are not an artifact. The analysis is then extended to the complete atmospheric diabatic heating by precipitation, radiation and surface fluxes to examine how the changing distribution of tropical weather states alters the convection–wave interactions and how the wave interaction changes the nature of the convection. Finally, section 4 summarizes our results and conclusions.

2. Datasets and methodology

a. Data sources

Our study is based on five data sources (Table 1): the ISCCP gridded cloud product (D1), the National Centers for Environmental Prediction–National Center for Atmospheric Research (NCEP–NCAR) reanalysis (NCEP-1), the Global Precipitation Climatology Project daily product (GPCP 1-DD), the ISCCP radiative flux profile product (ISCCP-FD), and the Goddard Surface Turbulent Flux Version 2 (GSSTF2). To analyze the cloud regimes as in Rossow et al. (2005), we use the ISCCP D1 product (Rossow and Schiffer 1999), which provides joint histograms of CTP (seven intervals) and optical thickness (τ; six intervals) over the period 1983–2004. The NCEP-1 reanalysis (Kalnay et al. 1996) is used to describe the atmospheric state (temperature and humidity) and winds at nine pressure levels at 6-h intervals for the same time period. Shorter records from 1997 to 2004 are used for studying the energy exchanges; daily atmospheric latent heating is obtained from the GPCP 1-DD (Huffman et al. 2001) and atmospheric and 3-hourly surface radiative heating are obtained from ISCCP-FD (Zhang et al. 2004). Daily ocean surface turbulent fluxes are obtained from GSSTF2 for the period 1989–2000 (Chou et al. 2003). Thus, we have a complete description of the variations of energy transfer to the atmosphere over the period 1997–2000.

The results are shown as 5-day (pentad) averages of all quantities. We found that the pentad averages provide more statistically robust results, despite some loss of temporal resolution. However, the cloud regime composites

TABLE 1. Primary data sources used in this study.

	ISCCP D1	NCEP-1	GPCP 1-DD	ISCCP-FD	GSSTF2
Variables	CPT–tau	Dynamic	Precipitation	Radiative net fluxes	Surface fluxes
Space resolution	2.5° × 2.5°	2.5° × 2.5°	1° × 1°	2.5° × 2.5°	1° × 1°
Vertical levels	Cloud regimes	1000, 925, 850, 700, 600, 500, 400, 300, 200 mb	Surface	TOA, surface, and atmosphere	Surface
Time resolution	3 h	6 h	Day	3 h	Day
Temporal domain available	1 Jul 1983–30 Jun 2008	1 Jan 1948–present	10 Oct 1996–30 Apr 2008	1 Jul 1983–31 Dec 2006	1 Jul 1987–31 Dec 2000
Temporal domain used	1 Jul 1983–31 Dec 2004	1 Jan 1983–31 Dec 2004	1 Jan 1997–31 Dec 2004	1 Jan 1997–31 Dec 2004	1 Jan 1989–31 Dec 2000

are constructed using daily datasets, particularly for precipitation, to preserve the correlations among the quantities—when we tried to use the 5-day averages directly, the results were significantly distorted.

b. ISCCP cluster analysis

The cluster analysis of the ISCCP D1 CTP–τ joint histograms defines six tropical weather states (WS) for the whole tropics (15°S–15°N) over 21.5 years (1983–2004) as shown in Fig. 1 (previously published by Rossow et al. 2005). Three correspond to active deep convection as indicated by the presence of high-topped, very optically thick clouds (WS1), cirrostratus (mesoscale) anvils (WS2), and smaller (unorganized) deep convection with midlevel cumulus congestus (WS3). Three other regimes represent convectively suppressed regimes: cirrus with some cumulus (WS4), shallow trade cumulus (WS5), and marine stratocumulus (WS6). There is a seventh regime corresponding to completely clear sky over the whole 280 km region (WS7), which is very rare. More details about these weather states can be found in Rossow et al. (2005).

The composite RFO (in %) of the convectively active WS are depicted in Fig. 2 as a function of longitude. The most frequent convective activity occurs in the 60°E–180° Indo-Pacific region where the RFO is almost twice that at other longitudes, around 25% on average for WS1 and WS2 together. In contrast, WS3 is more uniformly distributed, except for a minimum in the east Pacific and a maximum over South America. In the Indo-Pacific region, there is a minimum RFO for the suppressed cloud regimes (not shown). In agreement with Jakob and Schumacher (2008), WS6 is very rare (RFO = 2%) in the tropical western Pacific (130°–170°E).

c. MJO index

1) DATA

Several MJO indices have been used in the past to define an MJO cycle (Maloney and Hartmann 1998; Wheeler and Hendon 2004; Tian et al. 2006; Chen and Del Genio 2008). To look at the evolution of the WS as a function of the MJO phase, we need an index that does not depend on cloud- or precipitation-related quantities. We use the Chen–MJO index (Chen and Del Genio 2008) to estimate the date (in pentads) that the peak of an MJO event occurs at each longitude because this index is based only on the large-scale circulation indicated by anomalies of the velocity potential at 200 hPa from National Oceanic and Atmospheric Administration/Climate Prediction Center(NOAA/CPC). This choice also facilitates comparison to and extension of the results reported by Chen and Del Genio (2008) concerning the distribution of WS over MJO phase. This index is available online from the National Oceanic and Atmospheric Administration's Climate Prediction Center (http://www.cpc.noaa.gov/products/precip/CWlink/daily_mjo_index/pentad.shtml).

The Chen–MJO index is given at 10 locations centered at 20°, 70°, 80°, 100°, 120°, 140°, and 160°E and 120°, 40°, and 10°W. Negative values of the index represent enhanced convection, while positive values correspond to suppressed convection. In their study, Chen and Del Genio (2008) assumed that a strong MJO event is indicated by a negative index <-1. Other authors have followed this procedure but there has not been a systematic study of which criterion should be used to define an MJO event. Moreover, Chen and Del Genio (2008) focus on the Indo-Pacific warm pool and the boreal winter (November–April) period since the MJO convective activity seems to be most active in this region during this season. What about the MJO activity in other parts of the tropics or during the boreal summer (May–October) period? What does the MJO index look like over the whole year?

2) INDEX THRESHOLD

The evolution of the RFO of the MJO index values in three different intervals versus month is shown in Fig. 3. The black dashed line with square symbols corresponds to a threshold <-1 and >-1.4 and shows that there is an MJO signal (RFO at each location of around 9%) at

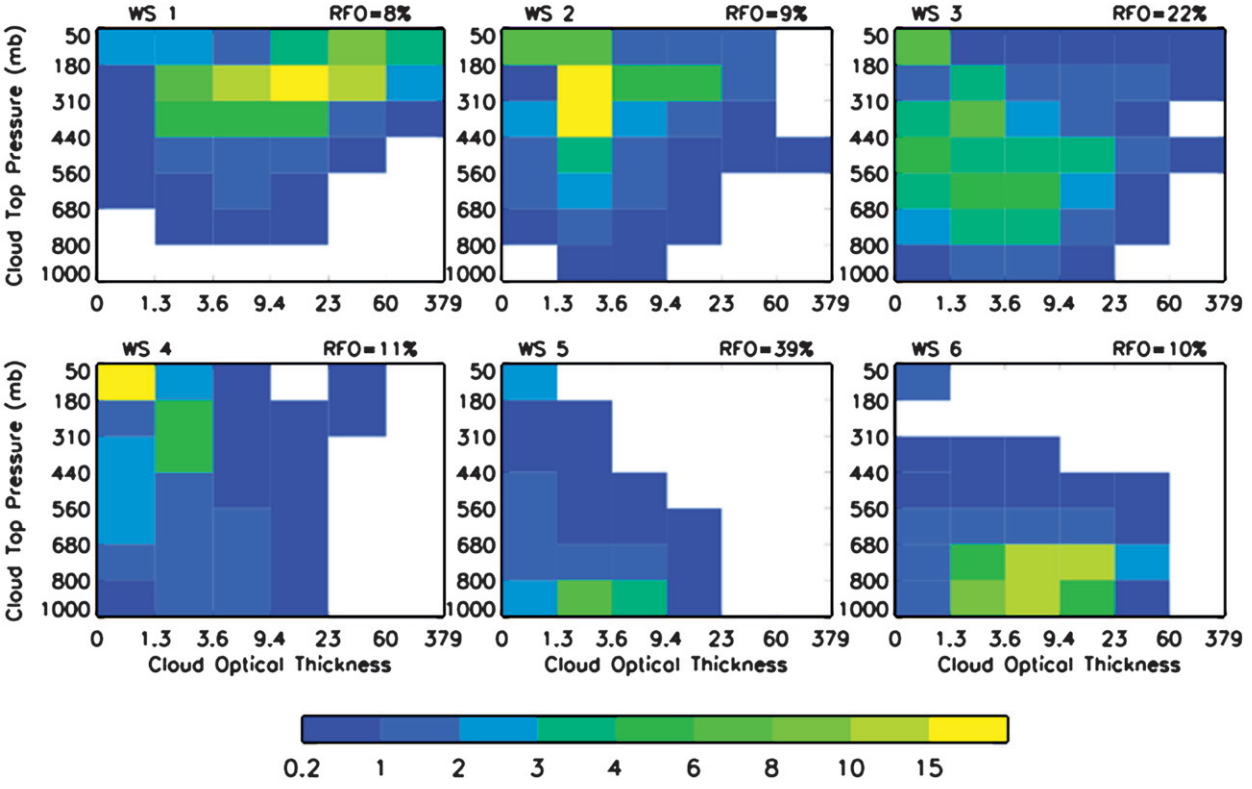

FIG. 1. Mean CTP–TAU histograms of six weather states from 3-hourly ISCCP D1 data over the tropical region of 15°N–15°S averaged over the period 1983–2004. The RFO (in %) is given for each weather state (Rossow et al. 2005).

some location all the time over the year, not just in the boreal winter. When averaged over all longitudes and years, the number of such events per year is about 10. These results mean that an MJO is not an ''on or off'' event but a constant signal that only varies in strength.

This result is consistent with evidence presented by some authors (i.e., Knutson and Weickmann 1987) for a continuous, global circumferential propagation of the MJO signal along the equator evident in the upper-level wind field as an atmospheric response to convective perturbations. According to Milliff and Madden (1996) and Matthews (2000), the MJO signal in wind and pressure continues to propagate farther east of the Indo-Pacific sector. We looked at the wind field in the lower and upper atmospheres (not shown) and found an eastward-propagating signal as in these previous studies, but the convective signal of the MJO is confined mainly to the Indo-Pacific region (60°E–180°) (cf. Zhang 2005). The MJO cycle in convection begins over the Indian Ocean and breaks down over the mid-Pacific Ocean (cf. Wheeler and Hendon. 2004). Looking at the precipitation fields, the signal is really concentrated in this sector (not shown). So we focus our study over the Indo-Pacific warm pool (60°E–180°), where the strongest convective activity occurs (Fig. 2).

If we decrease the index threshold below −2.6 (Fig. 3, dashed line with star symbols), these stronger MJO events occur almost exclusively during boreal winter. We could choose this threshold to define a strong MJO event. However, if we look at the solid line, where index threshold is <-2.2 and >-2.6, the trend of this line still shows a decreasing RFO from January to December (black arrow). So, considering the index sampling and in order to get enough MJO events for our study, we define strong MJO events as those during the boreal winter with an index value <-2.2 and weak events by index values <-1 but >-2.2 and compare results between strong and weak MJO events. In the next section we show additional evidence supporting this choice.

3. Tropical cloud regimes in the context of the MJO

a. *Characterization of organized and disorganized convection*

1) RELATIVE FREQUENCY OF OCCURRENCE OF CLOUD REGIMES

Composite RFO of the WS at seven lag times (in pentads) with respect to the MJO phase are obtained for both weak (Fig. 4a) and strong (Fig. 4b) MJO cases in

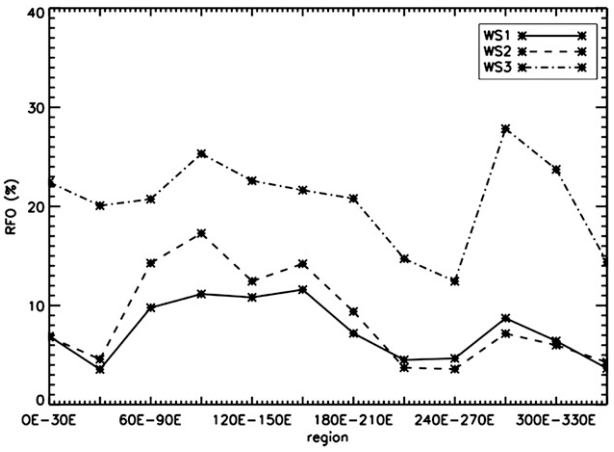

FIG. 2. Composite RFO (%) in the tropics (15°N–15°S) as a function of longitude sorted by convectively active weather states over the period 1983–2004: WS1 + 2: solid line; WS3: dashed line.

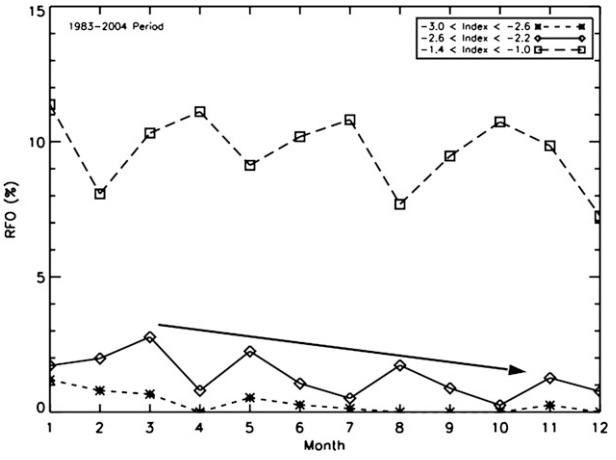

FIG. 3. Relative frequency of occurrence of MJO index interval as a function of month in the Indo-Pacific region (60°E–180°) averaged over the period 1983–2004.

the Indo-Pacific region (60°–180°) within a 5°N–5°S latitude band over November–April in the period 1983–2004. This domain is divided into six longitude zones of 20° with center longitudes the same as those used for the MJO index. The peak phase of MJO events is determined near the center longitude of each zone based on the occurrence of MJO index values <-1 but >-2.2 (weak) and values <-2.2 (strong). Lag 0 refers to a period of ± 2.5 days around the peak phase. Negative lag precedes the MJO peak in time or, equivalently, east of the peak wind anomaly. Chen and Del Genio (2008) selected the eight strongest MJO events in four November–April periods between 1999 and 2003. Our composites are formed from 277 weak MJO events and 35 strong MJO events in the period 1983–2004. We emphasize that the strong MJO events are not counted in the number of weak MJO events.

The RFOs of the deep convection (WS1) and anvil (WS2) regimes increase gradually up to the peak phase of the MJO (lag 0); the RFO of WS1 decreases dramatically at lag 1 (after 5 days) in the strong MJOs, while the occurrence of WS2 reaches its maximum at lag +1. In contrast, the smaller-scale convection with midlevel congestus (WS3) and the stratocumulus and shallow cumulus regimes (WS5/6) dominate several weeks before the MJO peak, decreasing to the peak and increasing after it. The RFO of the cirrus regime (not shown) is almost constant with MJO phase, suggesting that the presence of isolated cirrus is not dynamically associated with convective activity. This result is consistent with the results of Chen and Del Genio (2008) and with the finding by Luo and Rossow (2004) that more than half of the tropical cirrus is formed in situ well away from convection.

Figure 4 shows clearly the enhancement of mesoscale convective activity during MJO events as suggested by Mapes et al. (2006). The main difference in behavior between the two MJO strength categories is that the magnitude of the RFO increase of WS1 and WS2 at the peak is much larger (by 10%) in the strong cases than in the weaker cases, The suppressed regimes' decrease is also more dramatic in the strong cases. Since WS3 which also includes some isolated deep convection, has a larger RFO out of phase with the MJO, these results suggest that deep convection does not have an ''on/off'' behavior during an MJO event but rather changes character from less to more organized on the mesoscale. As we will see, the more organized convection is much more effective producing precipitation.

2) RELATIVE PEAK RATIO AND MJO INDEX THRESHOLD

To refine the relationship between deep convection and the MJO, we plot the ''peak ratio'' (PR) as a function of the MJO index threshold: the peak ratio for each WS is the ratio between RFO at the MJO peak phase (P_0 at lag 0) and the average RFO at lag -3 and lag $+3$ (P_{-3} and P_{+3}, respectively):

$$\mathrm{PR} = \frac{2P_0}{P_{-3} + P_{+3}}. \tag{1}$$

Figure 5 shows the values of PR for each cloud regime as a function of the MJO index (values are determined at intervals of 0.1 in a sliding window of 0.4). There is a relatively linear evolution of peak ratios for all WS. For WS1 and WS2 together, there is a hint of nonlinear behavior for MJO indices below -2.2 but the number of

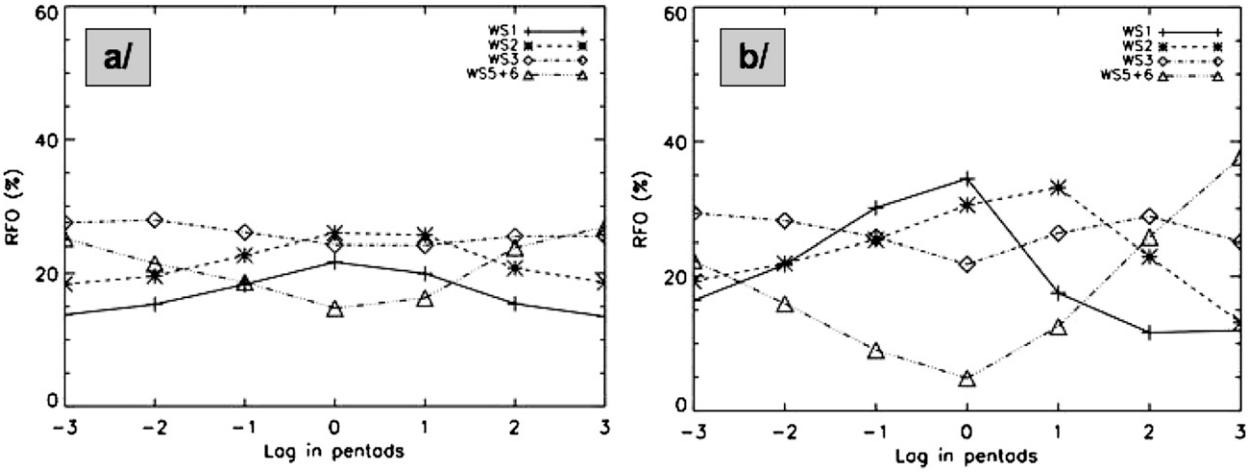

FIG. 4. Composite relative frequency of occurrence of cloud regimes formed at seven lag time (in pentads) with respect to the MJO phase in the Indo-Pacific region (60°E–180°) within 5°N–5°S latitude band averaged over November–April periods from 1983 to 2004 for both (a) weak and (b) strong MJO cases.

available cases is too small to be sure (there is a corresponding hint of enhanced WS5 and WS6 for MJO indices above +2). Although there is no distinct MJO index value corresponding to a strong event, the hint of a change of behavior at index of −2.2 as the threshold for strong MJOs is consistent with the discussion of Fig. 3 in the previous section. Note also that MJO index = −1, widely used by other researchers, is the value at which PR for WS1 and WS2 increases above unity and the value of PR for all the other WS falls below unity. This provides a more objective criterion to indicate an active MJO event, including discriminating between weak and strong events.

3) COMPOSITING METHOD

All the variables (V_{ij}), representing the atmospheric state and dynamics, as well as components of the atmospheric diabatic heating (precipitation, radiation, surface fluxes), are composited by cloud regime (index i) and MJO phase (index j). The relative frequency of occurrence (RFO_{ij}) of each combination is also obtained. Then the mean value of each variable at each MJO phase (AV_j) can be calculated by

$$\mathrm{AV}_j = \frac{\sum_{i=1}^{N_{\mathrm{ws}}} [\mathrm{RFO}_{ij} \times V_{ij}]}{\sum_{i=1}^{N_{\mathrm{ws}}} \mathrm{RFO}_{ij}}, \quad \text{with } N_{\mathrm{ws}} = 7. \qquad (2)$$

An interesting alternative is to assume that all these quantities vary only with WS and not with MJO phase so that only the WS RFOs vary with MJO phase (Fig. 4); in other words, that the relationships among the variables and the WS are independent of the MJO. Using this assumption, we can calculate the average variables (V_i^*) for each weather state by

$$V_i^* = \frac{\sum_{j=1}^{N_{\mathrm{Lag}}} [N_{ij} \times V_{ij}]}{\sum_{j=1}^{N_{\mathrm{Lag}}} N_{ij}}, \quad \text{with } N_{\mathrm{Lag}} = 7, \qquad (3)$$

and then determine the average value of a variable at each MJO phase (AV_j^*) by

$$\mathrm{AV}_j^* = \frac{\sum_{i=1}^{N_{\mathrm{ws}}} [\mathrm{RFO}_{ij} \times V_i^*]}{\sum_{i=1}^{N_{\mathrm{ws}}} \mathrm{RFO}_{ij}}. \qquad (4)$$

If $\mathrm{AV}_j^* \approx \mathrm{AV}_j$, then the WS composite variable values do not vary (much) with MJO phase; a significant difference indicates that the relationship of the variable and the WS changes with MJO phase. Comparison of the results obtained using both methods shows that the quantities that depend most directly on clouds (precipitation and radiation) have $\mathrm{AV}_j^* \approx \mathrm{AV}_j$, although the amplitude of the variation with MJO phase is usually a bit larger for AV_j. That the radiation depends much more on WS than MJO phase is not a surprise since the WS are defined by cloud (radiative) properties, but we find that precipitation is also more dependent on WS than MJO phase. In contrast, the relationship of the WS

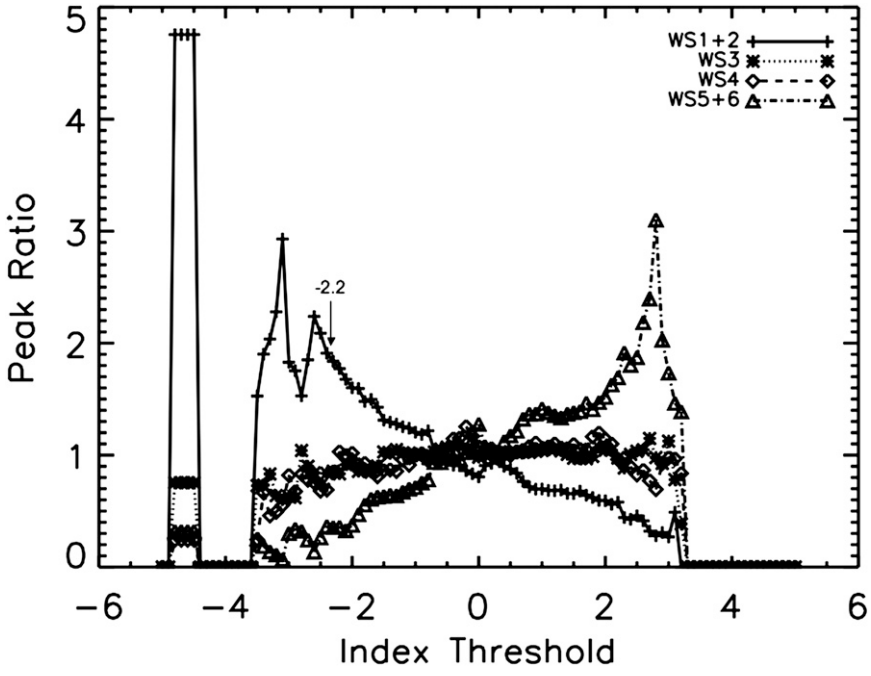

FIG. 5. Peak ratio of each cloud regime as a function of index threshold in the Indo-Pacific region (60°E–180°) within 5°N–5°S latitude band averaged over November–April periods from 1983 to 2004.

to the large-scale dynamical quantities, particularly the winds, is noticeably different using the first compositing method than when using the second. In particular, the vertical velocity in the midtroposphere and the onset time of the westerlies vary with compositing method. We return to a discussion of this point below while describing the detailed results of the compositing analysis using the first method.

b. Large-scale features of the MJO

We evaluate the quality of the NCEP–NCAR reanalysis data by looking at how it depicts the large-scale circulation features of the MJO. In particular, we want to make sure that weak MJOs observed in our analysis are not artifacts. We also want to show the basic variation of the atmosphere, even though it has been shown by others, to make clearer the connection between the variations of the WS and diabatic heating and the large-scale circulation.

1) HORIZONTAL WINDS

Time–longitude total zonal wind anomaly composites are obtained in Fig. 6a from NCEP-1 at 850 mb for weak MJOs relative to zero lag at three different locations [80°E (top), 120°E (middle), and 160°E (bottom)]. The solid bold black line indicates the zero anomaly contour, separating easterly and westerly wind anomalies. The MJO propagation is clearly present and tracks the precipitation anomalies from GPCP (Fig. 6b). The wind and precipitation anomaly patterns (not shown) are the same for the more numerous weak MJO events in boreal summer (313 versus 277 in winter) and for all strong MJO events, which are more numerous in boreal winter (35 versus 20 in summer). As in previous analyses of MJO (e.g., Lin and Johnson 1996; Houze et al. 2000; Kiladis et al. 2005), a more complete analysis of composite wind anomalies (not shown) reveals a vertical tilt involving a low-level westerly onset region below upper-level easterlies (Majda et al. 2007), westerly wind being present in a deep layer from the eastern Indian Ocean to the date line (Kiladis et al. 2005). These results confirm our conclusion that there is a ubiquitous MJO-like signal in the Indo-Pacific sector of the tropics, which varies in strength.

As in previous studies (Kiladis and Weickmann 1992; Kiladis et al. 2005; Gutzler et al. 1994; Tung and Yanai 2002), there is a vertical shear in the composite zonal wind anomaly cross sections in Fig. 7 for both weak (Fig. 7a) and strong (Fig. 7d) MJO cases. The vertical shear is a bit weaker for weak MJOs (for instance, anomalies decrease by around 50% at lag 1 at 700 mb, while anomalies stay about the same at 200 mb), which suggests that magnitude of the zonal wind shear is also related to the strength of the MJO signal. When we composite the zonal winds by cloud regime and allow only the variation of their RFO with MJO phase, the anomalies are much

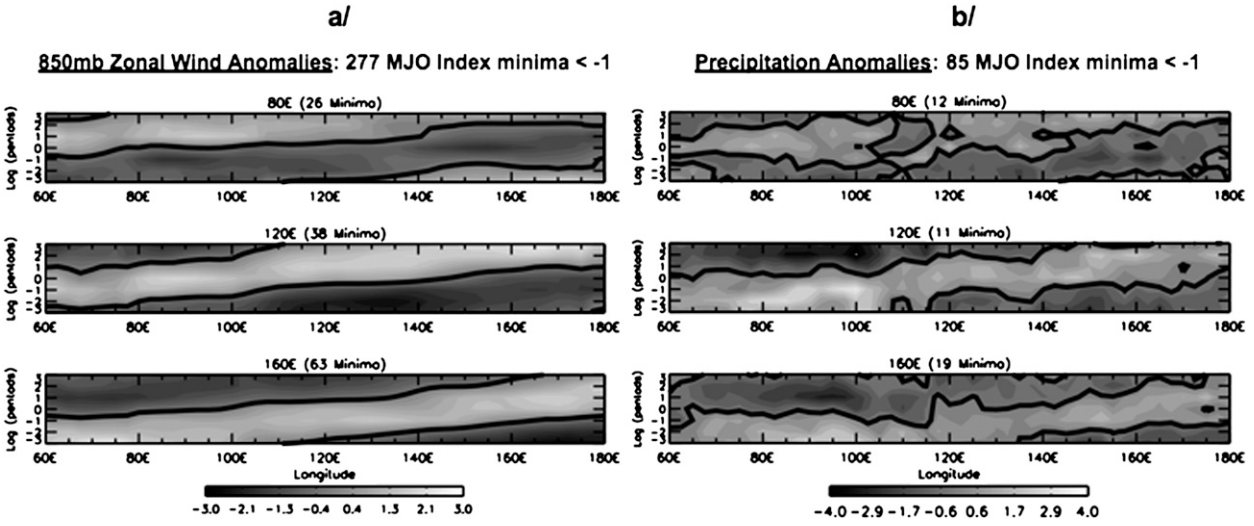

FIG. 6. Time–longitude anomaly composites for weak MJO in the Indo-Pacific region (60°E–180°) within 5°N–5°S latitude band averaged over November–April periods at three different locations centered at lag 0 (80°, 120°, and 160°E). (a) Total zonal wind anomalies at 850 mb (m s^{-1}); (b) total precipitation anomalies (mm day^{-1}).

weaker and show almost no vertical shear, in contrast to Fig. 7. This difference implies that compositing by WS alone mixes different MJO-dependent relationships between the WS and the large-scale circulation changes. Composite meridional wind anomalies (not shown) show no clear dependence on MJO phase (consistent with Zhang 1996); however, we note a vertical shear during an MJO life cycle in both weak and strong MJO cases, suggesting the presence of mixed Rossby–gravity waves as shown by Wheeler et al. (2000) and Yang et al. (2003). Using 40-yr European Centre for Medium-Range Weather Forecasts (ECMWF) Re-Analysis (ERA-40) data, Benedict and Randall (2007) showed that model simulations of MJO waves have meridional wind anomalies associated with such Rossby wave circulations. Thus, the MJO events begin with a weakening of the prevailing easterly winds eventually turning to westerly flow.

2) VERTICAL VELOCITY

Composite omega anomaly cross sections are shown in Fig. 7 as a function of the MJO phase for both weak (Fig. 7b) and strong (Fig. 7e) cases. The maximum upward anomalies occur slightly before lag 0, with the largest negative values occurring at the 400–500-hPa pressure level. This coincides with stronger organized convection (WS1 and WS2) before and at the MJO peak (see Fig. 4). For strong MJOs (Fig. 7e), upward motion anomalies begin strengthening in the lower troposphere almost 15 days prior the peak of the MJO during the time of increasing RFO for WS1. Slightly later the upward anomalies start to increase in the upper troposphere. A notable difference between weak and strong MJO is that the downward anomaly at the 700-hPa level never quite disappears for the weaker MJO, despite the fact that this anomaly is initially stronger for strong MJOs. The vertical motion anomalies become downward within a few days after the peak of the MJO, reaching largest downward anomalies at lag +2. The omega anomalies follow the variations of the WS1 RFO (Fig. 4) closely, where the RFO decreases dramatically 5 days after the peak of convection. Again, if we composite omega by cloud regime and only allow their RFOs to vary with MJO phase, we get approximately the same pattern of anomalies but the magnitudes are smaller. The fact that the NCEP reanalysis wind anomalies track the independently determined WS variations is confirmation of the realism of the NCEP reanalysis, which is also consistent with the ERA-40–based results of Benedict and Randall (2007). These results show that the upward motion anomalies lag the initial moistening at lower levels and gradually deepen as convection strengthens (as judged by increasing frequency of WS1 occurrence and its associated precipitation intensity).

3) SPECIFIC HUMIDITY

Anomalies in specific humidity for both weak (Fig. 7c) and strong (Fig. 7f) MJO events are more constrained by observations in the reanalysis than advective transports. The evolution of specific humidity anomalies (shown as departures from the MJO background state normalized by the mean state values) is consistent with Benedict's ERA-40 results (Benedict and Randall 2007): relatively drier air is prevalent throughout much of the troposphere in the convectively suppressed phase at the beginning of

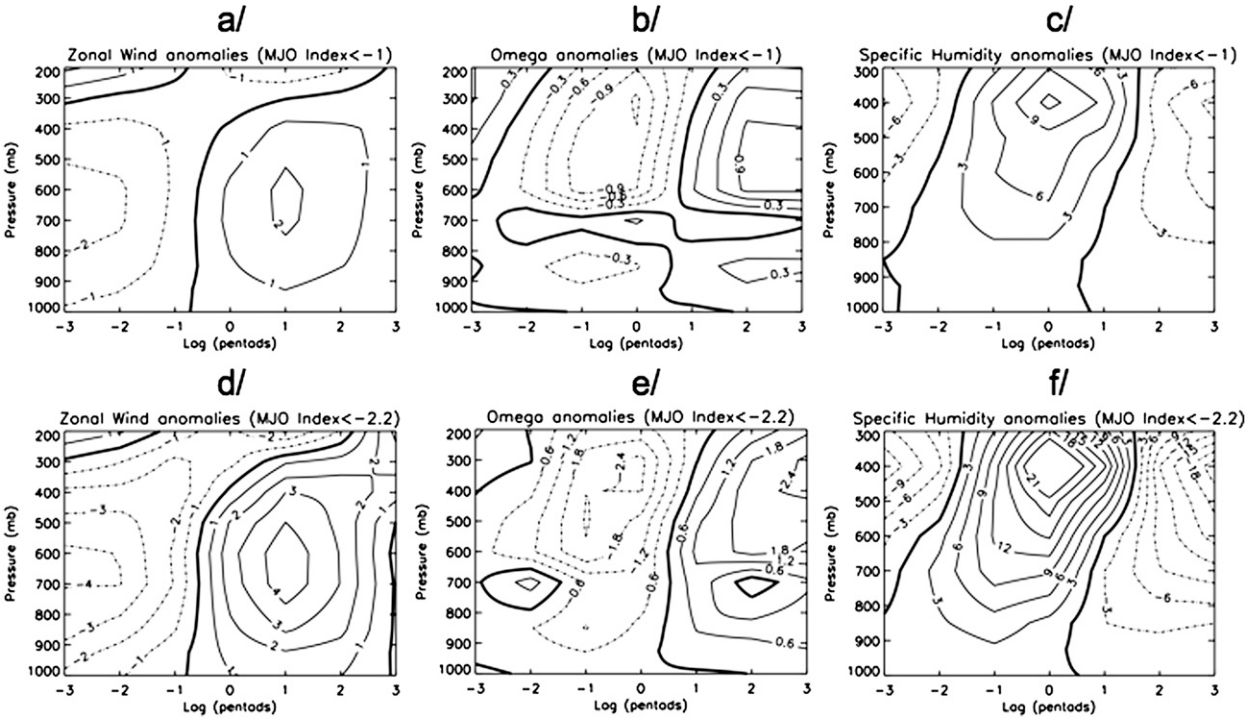

FIG. 7. (a),(d) Composite total zonal wind (m s^{-1}); (b),(e) omega (Pa $s^{-1} \times 100$); and (c),(f) specific humidity (%) anomaly cross sections as a function of the MJO phase in the Indo-Pacific region (60°E–180°) within 5°N–5°S latitude band averaged over November–April periods from 1983 to 2004. (a)–(c) Weak MJO case; (d)–(f) strong MJO case.

the MJO cycle. Beginning around −15 days, weak, shallow moistening develops in the lower troposphere coincident with weakening of the easterly winds. The moist anomalies strengthen and deepen up to the 600-hPa level between days −15 and −10, coincident with weak rising motions and with a relatively large RFO of WS3. Figure 4 shows declining shallow cumulus and constant WS3, midlevel congestus, during this period. As the lower and middle troposphere moistens, convection switches from WS3 to WS1/WS2 along with increasingly strong upward motions. By lag 0, the convective precipitation has reached its maximum along with upward motions; maximum positive moisture anomalies now appear at the 400-hPa level, likely because of transport by the strong deep convection. Note that the maximum upward omega anomaly appears just before the maximum moistening; in fact, the upper levels remain moister than the average for five more days, coinciding with the peak RFO of WS2, the anvil clouds (Fig. 4).

Beginning around 2–3 days after the peak convection, drier air intrudes into the lower troposphere and then expands into the middle and upper troposphere over the next 5–7 days. This evolution of the specific humidity anomaly profile is consistent with Benedict's ERA-40 results (Benedict and Randall 2007) as well as with the findings of many studies based on radiosonde data (Lin and Johnson 1996; Kiladis et al. 2005) and remotely sensed vapor measurements (e.g., Myers and Waliser 2003). The dry air intrusion also coincides with a dramatic decrease in WS1 RFO, especially for strong MJOs. Thus, using the NCEP–NCAR reanalysis, we find the same progression as in previous studies (Maloney and Hartmann 1998; Stephens et al. 2004; Kiladis et al. 2005; Benedict and Randall 2007): from suppressed conditions dominated by shallow convection and a drier upper troposphere, through gradual lower-tropospheric moistening, increasing frequency of mesoscale deep convection (WS1), followed by decaying anvil clouds (WS2) and upper-level moistening, and a final stabilization during the period of the westerly anomaly of the zonal wind when dry subtropical intrusions once again suppress deep convection.

c. *Variation of energy transfer to the atmosphere*

1) PRECIPITATION

To diagnose the interaction between the large-scale MJO wave and deep convection, we analyze the evolution of the complete atmospheric diabatic heating during MJO events. Each WS1 (mesoscale deep convection) produces 3 and 4 times more precipitation, around 18 mm day^{-1} on average, than WS2 and WS3 respectively (not shown).

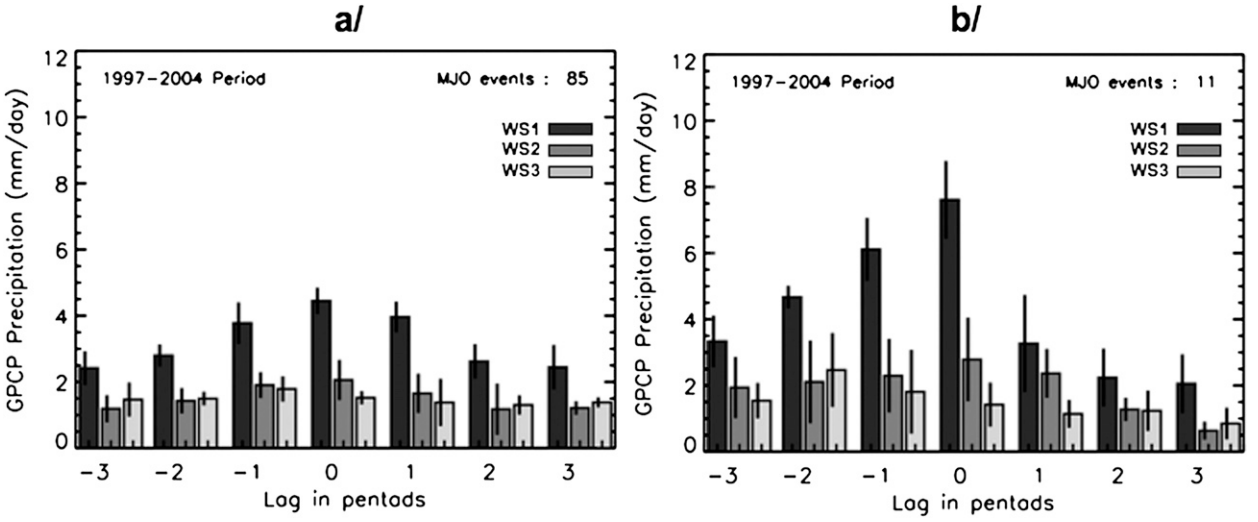

FIG. 8. Composite GPCP precipitation (mm day^{-1}) for each cloud regime as a function of the MJO phase in the Indo-Pacific region (60°E–180°) within 5°N–5°S latitude band averaged over November–April periods from 1997 to 2004. (a) Weak MJO case; (b) strong MJO case.

This relationship is nearly uniform in longitude and season and independent of MJO phase. WS1 and WS2 (anvil clouds) vary together so that variations of tropical rainfall are clearly dependent on the RFO of these two weather states.

Composites of GPCP precipitation as a function of the MJO phase for convectively active WS (precipitation being under 0.5 mm day^{-1} for the others) are depicted in Fig. 8 for both weak (Fig. 8a) and strong (Fig. 8b) MJOs. There are 85 weak events during this period and 11 strong events. The vertical black lines correspond to the standard deviation of precipitation among these events. In general, the RFO of WS3 is larger than that of WS1 in the tropics so that the total precipitation produced by each is nearly the same. However, the variation of precipitation during MJO is clearly associated with the change from WS3 to WS1, consistent with Jakob and Schumacher (2008). During stronger MJOs, the increase of WS1 and decrease of WS3 are both greater in magnitude.

The evolution of total precipitation anomaly as a function of the MJO phase is shown in Fig. 9 with the mean value over all lags, given in the upper-left corner and the standard deviation of precipitation among events represented by error bars (large base for strong MJO events). On average, strong MJO events produce only about 1.2 mm day^{-1} (≈8%) more precipitation than weak MJO events, but the variation of precipitation intensity over the MJO cycle is much larger (≈7 mm day^{-1}) than for weak events (≈2 mm day^{-1}). The small variation of total precipitation is associated with the offsetting RFO and individual precipitation rates for WS1 and WS3, suggesting a reason why weaker MJO events have not been recognized without this separation. Positive anomalies appear about 10 days before the MJO peak anomalies and disappear about 5 days after the peak. As expected (since the MJO was first recognized in precipitation measurements), total precipitation anomalies peak at MJO phase lag 0, increasing before this peak and decreasing after it. For the stronger MJOs, these anomalies display a distinct temporal asymmetry: precipitation increases steadily for the 15 days preceding the peak and drops sharply in the 5 days after the peak. Note, however, that the contribution from WS2 does not decrease

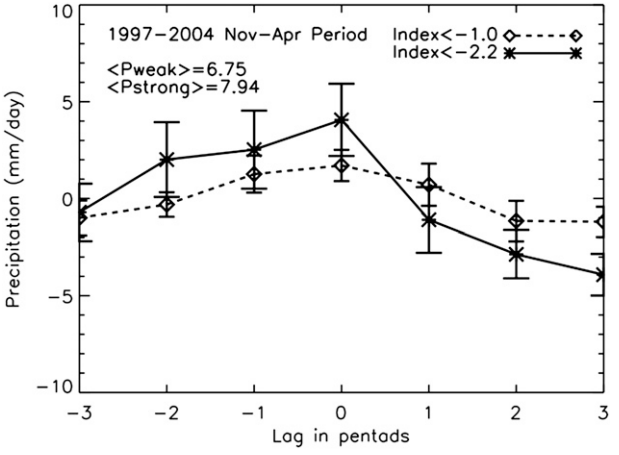

FIG. 9. Composite total GPCP precipitation anomalies (mm day^{-1}) as a function of the MJO phase in the Indo-Pacific region (60°E–180°) within 5°N–5°S latitude band averaged over November–April periods from 1997 to 2004. Dashed line: weak MJO; solid line: strong MJO.

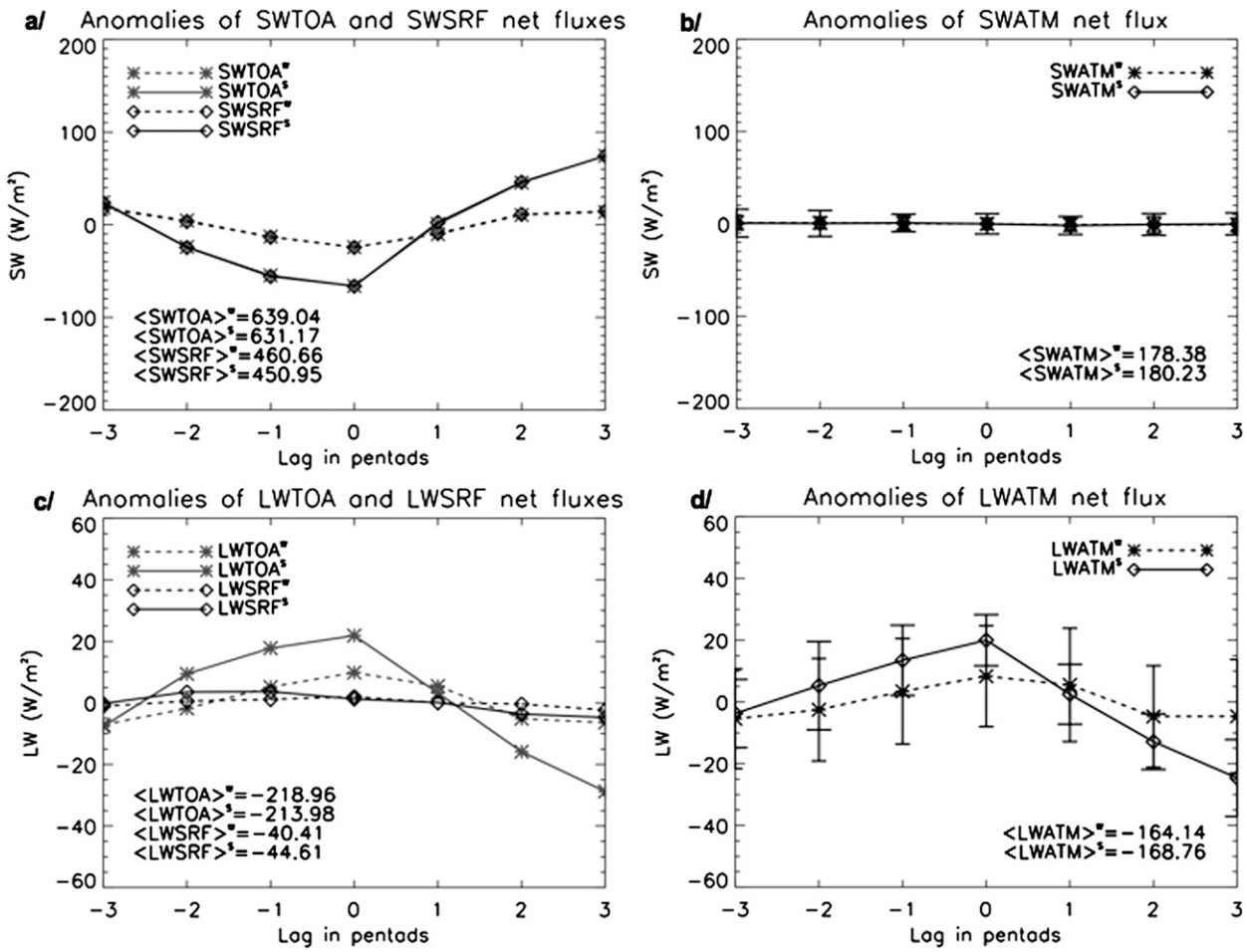

FIG. 10. Composite total radiative net flux anomalies (W m^{-2}) as a function of the MJO phase in the Indo-Pacific region (60°E–180°) within 5°N–5°S latitude band averaged over November–April periods from 1997 to 2004. (a) Full-sky shortwave net flux anomalies at the TOA and at the surface (SRF); (b) full-sky shortwave net flux anomalies in the atmosphere (ATM); (c) full-sky longwave net flux anomalies at the TOA and at SRF; and (d) full-sky longwave net flux anomalies in ATM. (a),(c) Star symbol: radiative net fluxes at the TOA; diamond symbol: radiative net fluxes at the surface; dashed line: weak MJO case; and solid line: strong MJO case.

until 10 days after the peak. Thus, the RFO of WS1 provides a more distinct MJO signal, even for the weak events.

2) RADIATIVE FLUXES AND HEATING

The composite variations of net shortwave (SW) and longwave (LW) radiative fluxes at the top of the atmosphere (TOA), at the surface, and in the atmosphere are shown in Fig. 10 (SW in Figs. 10a,b and LW in Figs. 10c,d). The radiative fluxes are essentially constant with longitude and season for a given WS since the WS are defined by the cloud optical properties. Moreover, there is a little variation of the net fluxes with WS except for TOA (and in the atmosphere) net LW, which varies with cloud-top height (not shown). Total in-atmosphere SW absorption is nearly the same for all WS because cloud effects are offset by water vapor effects (the exception is WS2, which has a SW absorption about 40 W m^{-2} smaller that for the others WS in the Indo-Pacific region); the cloud effects on SW radiative fluxes during an MJO event cool the ocean surface, but do not alter the total atmospheric heating. Longwave net fluxes, which cool the atmosphere, are systematically reduced by about 70 W m^{-2} as cloud-top height increases, going from convectively suppressed WS to convectively active WS. Note that the fair weather mixture of cirrus and cumulus (WS4) and the scattered convection–congestus mixture (WS3) have about the same radiative effect. Consequently, the transition from suppressed to disorganized to organized convection (WS1 and WS2) appears as a monotonic decrease in LW cooling of the atmosphere by about 20 W m^{-2}. Thus, cloud effects on radiation produce a heating of the atmosphere coincident with and reinforcing the precipitation heating.

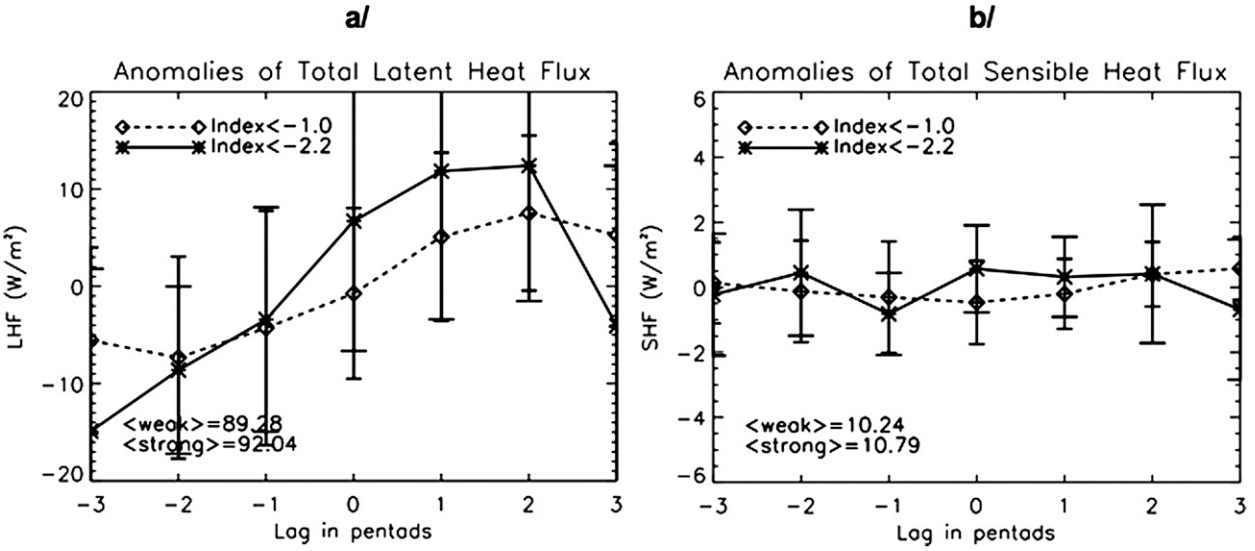

FIG. 11. (a),(b) Composite total latent (sensible) heat flux anomalies as a function of the MJO phase in the Indo-Pacific region (60°E–180°) within 5°N–5°S latitude band averaged over November–April periods from 1989 to 2000. Dashed line: weak MJO case; solid line: strong MJO case.

A subtle effect is that the changeover to more organized, mesoscale convection during an MJO leads to the increased occurrence of WS2, which in the strong events persists for a 5 days past the peak of the event (Fig. 4); this has the effect not only of prolonging the LW heating of the atmosphere but also of enhancing solar heating of the atmosphere which offsets decreasing latent heating somewhat.

Figure 10 also shows why the use of outgoing longwave radiation (OLR) (LW net flux at TOA) to detect anomalous events in the tropics is too insensitive to changes. Not only is the magnitude of the OLR variations for weaker MJO events very small, but the effects on these fluxes of WS3 and WS4, the latter not associated with convection, are nearly the same. Thus OLR variations do not provide as clear a signal for the occurrence of convection (WS3 and WS4 are hard to distinguish) nor do they capture the switch from disorganized to organized convection (WS3 transition to WS1). As Fig. 10 shows, use of OLR detects the stronger MJO events but may miss the weaker events.

3) SURFACE FLUXES

We composited surface latent and sensible heat fluxes as a function of longitude sorted by weather states (not shown). In general the surface fluxes exhibit a local minimum in the Indo-Pacific sector. The dependence of the latent and sensible fluxes on WS is weak except for the contrast between WS5 (boundary layer cumulus) and the other WS; hence, the variation of total surface fluxes over the MJO cycle is mainly due to relative variation of the RFO of this WS with respect to the others. Figure 11 shows the MJO composite latent (Fig. 11a) and sensible (Fig. 11b) heat flux anomalies as a function of phase. There is little variation of sensible heat fluxes (SHF) but a notable increase of surface latent heat flux (LHF) following the peak of the MJO events. The small SHF variation is explained by the weak SST variability over 20 days as shown by Woolnough and Slingo (2000). The latent heat flux variations are explained by anomalies of the specific humidity at 1000 mb (Fig. 12) that show a moistening of the lower troposphere in the 5–10 days

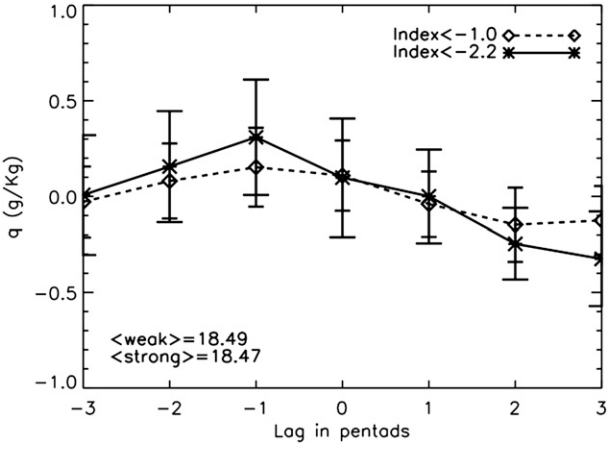

FIG. 12. Total specific humidity anomalies (%) at 1000 mb as a function of the MJO phase in the Indo-Pacific region (60°E–180°) within 5°N–5°S latitude band averaged over November–April periods from 1983 to 2004. Dashed line: weak MJO case; solid line: strong MJO case.

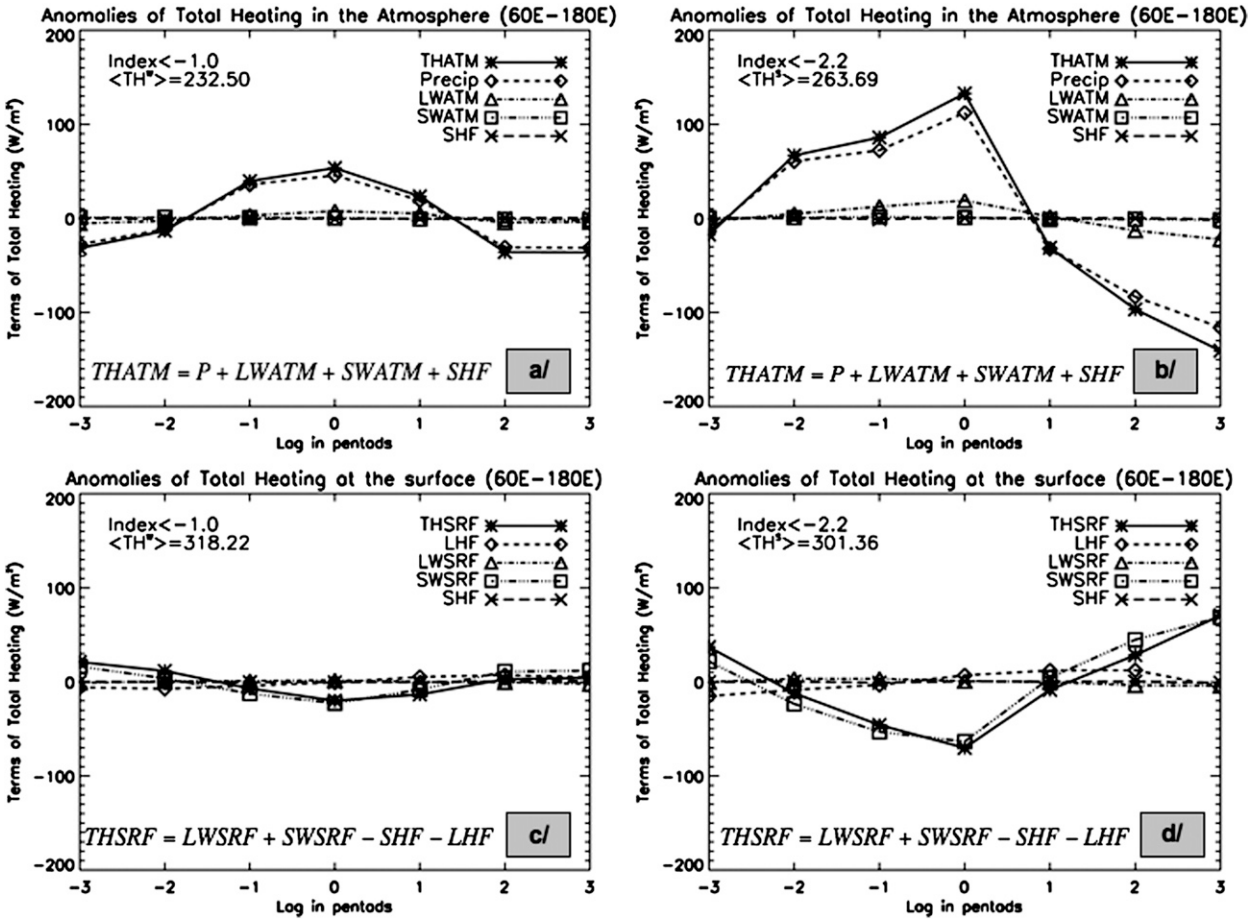

FIG. 13. Total heating anomalies (a),(b) in ATM and (c),(d) at SRF as a function of the MJO phase in the Indo-Pacific region (60°E–180°) within 5°N–5°S latitude band averaged over November–April periods in both weak [(a) and (c)] and strong [(b) and (d)] MJO cases. Precip: precipitation anomalies; LW: longwave net flux anomalies; SW: shortwave net flux anomalies; LHF: latent heat flux anomalies; SHF: sensible heat flux anomalies.

preceding the MJO and sudden drying after the peak. This drying, rather than enhanced surface winds (not shown), explains the increased surface latent heat fluxes following the peak of the MJO. The anticorrelated time evolution of latent heat flux and specific humidity anomalies during the MJO cycle, as well as the magnitude of the total precipitation, demonstrates that the local surface is not the source of the additional water vapor. In particular, the local evaporation amount has the same order of magnitude as the precipitation coming from WS 3–6 but is not sufficient for the precipitation coming from WS 1–2 by a factor of few. In agreement with Benedict and Randall (2007), we conclude that moistening must be caused by convergence of the horizontal winds (Fig. 7).

d. Total heating in the atmosphere and at the surface

We calculate anomalies of the total diabatic heating of the atmosphere, as well as the anomalies of the net heating of the surface, as a function of the MJO phase (Fig. 13) for both weak and strong events.

In the atmosphere, the total heating (THATM) is given by

$$\mathrm{THATM} = P + \mathrm{LWATM} + \mathrm{SWATM} + \mathrm{SHF}, \quad (5)$$

where P is precipitation, LWATM (SWATM) is the in-atmosphere LW (SW) net flux and SHF is the sensible heat flux. Since THATM is a linear sum of the components, its anomaly is just the sum of the anomalies of each component. The standard deviations of total heating terms are given in Table 2 (Table 3) for weak (strong) MJO case.

For both MJO cases, total heating of the atmosphere is mainly due to precipitation, reinforced by LWATM. SWATM and SHF play little role in the MJO energy cycle. Whether the diurnal modulation of convection and surface fluxes (the radiative fluxes are based on 3-hourly

TABLE 2. Standard deviation of total heating terms: weak MJO.

σ_{weak} (w.m^{-2})	Lag −3	Lag −2	Lag −1	Lag 0	Lag 1	Lag 2	Lag 3
Precip	26.9	19.1	27.7	23.5	32.1	30.2	23
LHF	12.6	11.8	13.5	10	10.6	11.6	12.4
SHF	1.5	1.7	1.8	1.3	1.2	1.3	1.2
LWSRF	7.2	7.2	7.6	7.2	7	6.8	6.6
SWSRF	28.7	25.6	26.2	26.3	28.9	32	25.3
LWATM	16.1	16.6	17	16.3	18.3	16.4	18.4
SWATM	7.7	6.5	7.3	6.1	6.9	8.6	7
THATM	32.3	26.2	33.4	29.3	37.6	35.4	30.3
THSRF	32.2	29.1	30.5	29	31.6	34.7	29

TABLE 3. Standard deviation of total heating terms: strong MJO.

σ_{strong} (w.m^{-2})	Lag −3	Lag −2	Lag −1	Lag 0	Lag 1	Lag 2	Lag 3
Precip	46	55.7	65.6	60	55.5	39.2	35.5
LHF	16.7	9	11.5	13.4	15.2	14.7	21.4
SHF	1.9	2	1.3	1.3	1.2	2.2	2.4
LWSRF	7.6	7.2	7.7	5.8	6.8	6.6	7.7
SWSRF	55.7	81	42.6	39.9	45.2	51.9	47.2
LWATM	11	14.3	11.4	8.3	9.7	9	12.4
SWATM	15	14	9.5	11	9.7	11.8	11.8
THATM	49	59	67.2	61.5	57.2	42	39.5
THSRF	58.7	81	44.8	42.5	48.2	54.4	52.4

results) changes these results significantly needs further investigation when higher time resolution surface flux data become available. Note that amount of precipitation (Figs. 13a,b) is more than an order of magnitude larger than the local evaporation (Figs. 13c,d), confirming the conclusion that the water for the precipitation is advected in from a much larger region and that the local surface evaporation plays little role in the atmospheric heating. Maximum total heating occurs at the MJO peak and is almost 3 times larger for strong MJOs than for weak ones. The atmosphere appears to have returned to its prior state about 15 days after the peak, whereas strong events exhibit a much larger suppression of precipitation even 15 days after the peak. The shape of the anomaly plots in Fig. 13 suggests that the variation of the length of MJO events may be caused, in part, by the difference in strength, where the weak events are only noticeable over a shorter time period. The areas under the curves give the total heating of the atmosphere: weak MJO events produce only a small net heating of the atmosphere (34 W m^{-2}), whereas strong MJO events produce a much larger net heating pulse (79 W m^{-2}). In others words, strong MJO events act to increase the heating of the atmosphere by nearly 50% of its mean value. A pulse of heating in the atmosphere was proposed by Lau and Peng (1987) and Wang and Xue (1992) to improve instability theories of the MJO (Zhang 2005).

At the surface, the total heating (THSRF) is given by

$$\text{THSRF} = \text{LWSRF} + \text{SWSRF} - \text{SHF} - \text{LHF}, \quad (6)$$

where LWSRF (SWSRF) is the LW (SW) net flux at the surface and LHF is latent heat flux (evaporation). In contrast with the atmosphere, surface cooling (heating) is enhanced before (after) the MJO peak, being mainly dependent on SW flux anomalies. Weak MJO events produce a small net cooling of the surface (−12 W m^{-2}), whereas strong MJO events produce larger net cooling response (−54 W m^{-2}). Although there are small SST anomalies associated with the MJO events (Woolnough and Slingo 2000), the surface energy exchanges appear to be a passive response directly linked to cloud radiative effects.

4. Discussion and concluding remarks

Although research on the MJO is currently in its fourth decade, many aspects of this tropical disturbance remain unsolved—including wave triggering mechanisms, extratropical connections, scale interactions, and cloud processes. The main goal of this study was to investigate the energy exchanges to elucidate the interaction between deep convection and the large-scale circulation associated with the MJO. The MJO index time record indicates the ubiquitous presence of an MJO-like signal in the Indo-Pacific sector of the tropics, especially in the wind anomalies, meaning that an MJO is not an ''on or off'' event but rather a signal that varies in strength. A MJO criterion based on weather states could be used to distinguish weaker or stronger MJOs. WS RFOs vary over the MJO cycle so as to suggest that deep convection changes character from less to more organized on the mesoscale during an MJO event. Compositing all the variables—representing the atmospheric state and dynamics variables, as well as components of the atmospheric diabatic heating—by cloud regimes, we found that precipitation and radiation anomalies depend only on WS, whereas WS RFOs depend on the large-scale circulation. In other words, the relationship of WS and the large-scale circulation varies over an MJO cycle.

The asymmetry of the variations of precipitation intensity over the MJO cycle provides a circumstantial argument for the interpretation that the large-scale dynamics causes the increased convection and not the reverse. Moreover, the evolution of the WS RFOs indicates that the large-scale wave moistens the lower troposphere and changes the type of convection from mostly WS3 to mostly WS1, from scattered, smaller-scale convection to larger, mesoscale convective systems. WS1-type convection is much more effective at converting the advected water vapor to precipitation.

Sorting surface fluxes by WS and MJO index shows that surface fluxes play little role in an MJO. Surface sensible fluxes do not vary significantly and contribute little to the atmospheric heating. Surface evaporation does not contribute significantly to moistening before the MJO peak and looks like it is a passive response to the atmospheric drying after the peak. This conclusion is reinforced by the fact that the precipitation anomaly is much larger than the local evaporation anomaly. The enhanced deep convection also appears to moisten the upper troposphere. The convective precipitation heating anomaly precedes the peak of MJO and shuts down after the peak. Although heating of the atmosphere comes mainly from precipitation heating, the longwave (and shortwave due to an increase in WS2) radiative effects of cloud changes reinforce it. Despite the large differences between deep cumulus, shallow cumulus, and cirrus clouds, radiation exhibits little variation in weak MJOs, and plays only a small role in the total budget of heat in the atmosphere. Overall, an MJO event produces a net heating of the atmosphere. During a weak event, the atmosphere returns to a near average state 10 days after the MJO peak, whereas a strong MJO event produces a strong heat pulse that is not immediately removed. Atmospheric kinetic energy (proportional to the square of the zonal wind, not shown) becomes about twice as large after the peak of the MJO implying that the net heating amplifies the wave. The ultimate balancing loss by radiation and advection must happen later or elsewhere.

In contrast, the total energy budget at the surface shows a net cooling by an MJO event. Local surface energy exchanges appear to be a passive response directly linked to cloud radiative and humidity variations. The atmospheric coupling to the ocean is not local but much larger scale in order to have the right time scale.

Thus the sequence of events in an MJO looks like 1) the large-scale wave humidifies the lower troposphere and reorganizes deep convection into mesoscale systems that are more efficient at producing precipitation, have larger radiative effects, and moisten the upper troposphere; 2) latent and radiative heating of the atmosphere occurs because of the mesoscale convection; 3) the large-scale wave shuts down convection by drying the lower troposphere; but 4) the large-scale circulation gains energy because of the convective heating.

In other words, the waves organize and amplify convection, which is always present, but there is a positive feedback loop in that this serves to amplify the wave. Is there more than one kind of convection and waves? We do not address the types of waves but Kiladis et al. (2005) analysis shows that there is more than one type. We have not explained where the wave comes from—extratropical source or creation of waves by variable heat sources by disorganized convection—but we definitely show that there is more than one style of convection, represented by WS1/WS2 and WS3. It is the change of style that constitutes an MJO event (cf. Mapes et al. 2006). The analysis is incomplete and needs to be extended by using the ISCCP convective tracking dataset (Rossow and Pearl 2007) along with CloudSat–Cloud-Aerosol Lidar and Infrared Pathfinder Satellite Observation (CALIPSO) to examine variations in vertical structure and to investigate their effects.

Clearly studies are needed to investigate how the large-scale waves organize the convection: merely moistening the lower and middle troposphere does not seem to be enough. Is there some additional process? The answer to this question could be related to the strength of the MJO. Why is a particular MJO event weak or strong? Is it due to an extratropical source of energy? Our analysis will need to be extended in a larger time window to take into account several MJO cycles in order to study connections between weak and strong MJO events. We would need to open our spatial window to the whole tropics as well since there is MJO activity in other parts of the tropics, outside the Indo-Pacific region. Why should the coupling between convection and waves be different in the Indo-Pacific region from the rest of the tropics? Using the MJO index and looking at zonal wind anomalies, we counted 28 strong MJO events for the period 1983–2004 outside this sector (35 inside the Indo-Pacific region). Why are there any strong MJOs outside this region?

As summarized in the introduction, a number of theories have been proposed to explain the MJO, but we still do not have a total understanding of this phenomenon. The results of our study make a contribution by refining the changes in convection and quantifying the energy exchanges. These facts should help modelers to refine theories and identify model shortcomings. The WISHE (Emanuel 1987; Neelin et al. 1987), the air-sea coupled intraseasonal interaction (ASCII) (Flatau et al. 1997), and radiative instability (Raymond 2001) theories are definitely contradicted by both the timing of surface latent heat flux (the anomaly maximum occurring after the MJO peak and not before) and the magnitude of latent heat flux (many times smaller than precipitation). As we showed, surface fluxes do not supply very much energy to the atmosphere. Raymond (2001) considered deep convective activity in the tropics as being proportional to the net energy input into the troposphere from the surface fluxes and radiation. Our data show that the radiative and surface flux anomalies are too weak compared to latent heating from precipitation. In the boundary layer, frictional convergence in front of the propagating convection might explain the moistening in

the lower atmosphere before the MJO peak as well as the drying occurring after the passage of convection with westerly wind perturbations. However, the scale of the convection may be wrong if it is limited to WS3. Possibly the transition from WS3 to WS1 reflects Moncrieff's momentum transfer process that couples convection to larger-scale waves. Such a dynamical process might be confirmed by combining the convective tracking dataset with vertical heating profiles and large-scale wind variations. Even if this theory does not explain the seasonality, it could account for the constant presence of the MJO signal. Wave-CISK, like the other proposed instability-type theories, seems contradicted by the constant presence of the signal and does not explain the seasonality. But it could be the ''amplification'' process. Combining both theories, the frictional wave-CISK via a stochastic linearized convection (Salby et al. 1994) produces seasonality in accord with observed. While sharing essential features with the MJO in the Eastern Hemisphere, this theory does not explain observed behavior in the Western Hemisphere where the convective signal is largely absent. Generating a planetary-scale linear response to moving heat sources, Chao (1987)'s model requires the propagating convection before the wave. Our amplification of the wave by convective heating might support this theory as part of the story but the MJO signal is already there and always there, so this might just be one stage in the next theory. Finally, extratropical wave forcing might provide the ''initial'' wave activity. This is supported by the seasonality (midlatitude storms are stronger and closer to the equator in boreal winter) and by the fact that the signal is always present. This idea would still need one of the other convection–tropical wave interaction theories (including CISK) to be complete. The extratropical source of energy might also play some role in differentiating between weak and strong MJOs.

Large-scale tropical waves and deep convection are usually assumed to be coupled because of the observed association between variations of the winds and OLR (Zhang 2005), but this association does not demonstrate a coupling per se nor elucidate the nature of this coupling (cf. Kiladis et al. 2005). Our study provides more direct evidence for a coupling, better than correlating OLR and wind anomalies, by diagnosing the energy exchanges explicitly. These (and other) results show that the large-scale waves change the organization of the deep convection and provide the extra moisture needed for the precipitation: the moistening appears first in the lower troposphere ahead of the net heating of the atmosphere by convection at the MJO peak. Following this pulse of heating by convection, atmospheric kinetic energy becomes much larger. As others have found, the signature of the MJO wave can be found in the wind field over the whole tropics, but the coupling to convection is confined mainly to the Indo-Pacific region. Why this is so remains an open question that needs to be the focus of the next investigations.

Acknowledgments. Authors thank Anthony Del Genio at NASA GISS for giving us the idea to initiate this study. E. Tromeur acknowledges NSF Funding of the Center for Multi-scale Modeling of Atmospheric Processes at Colorado State University and W. B. Rossow acknowledges NASA Grant NNXD7AN04G. NCEP/NCAR reanalysis data are provided by the NOAA/OAR/ESRL PSD, Climate Diagnostics Center, Boulder, Colorado, from their Web site at http://www.cdc.noaa.gov/.

REFERENCES

Benedict, J. J., and D. A. Randall, 2007: Observed characteristics of the MJO relative to maximum rainfall. *J. Atmos. Sci.,* **64,** 2332–2354.

Bladé, I., and D. L. Hartmann, 1993: Tropical intraseasonal oscillations in a simple nonlinear model. *J. Atmos. Sci.,* **50,** 2922–2939.

Chao, W. C., 1987: On the origin of the tropical intraseasonal oscillation. *J. Atmos. Sci.,* **44,** 1940–1949.

——, and B. Chen, 2001: The role of surface friction in tropical intraseasonal oscillation. *Mon. Wea. Rev.,* **129,** 896–904.

Chen, Y., and A. D. Del Genio, 2008: Evaluation of tropical cloud regimes in observations and a general circulation model. *Climate Dyn.,* **32,** 355–369, doi:10.1007/s00382-008-0386-6.

Chou, S.-H., E. Nelkin, J. Ardizzone, R. Atlas, and C.-L. Shie, 2003: Surface turbulent heat and momentum fluxes over global oceans based on the Goddard satellite retrievals, version 2 (GSSTF2). *J. Climate,* **16,** 3256–3273.

Emanuel, K. A., 1987: An air–sea interaction model of intraseasonal oscillations in the tropics. *J. Atmos. Sci.,* **44,** 2324–2340.

Flatau, M., P. J. Flatau, P. Phoebus, and P. P. Niiler, 1997: The feedback between equatorial convection and local radiative and evaporative processes: The implications for intraseasonal oscillations. *J. Atmos. Sci.,* **54,** 2373–2386.

Gutzler, D. S., G. N. Kiladis, G. A. Meehl, K. M. Weickmann, and M. Wheeler, 1994: The global climate of December 1992–February 1993. Part II: Large-scale variability across the tropical western Pacific during TOGA COARE. *J. Climate,* **7,** 1606–1622.

Hendon, H. H., and B. Liebmann, 1990: The intraseasonal (30–50 day) oscillation of the Australian summer monsoon. *J. Atmos. Sci.,* **47,** 2909–2924.

Houze, R. A., Jr., S. S. Chen, D. E. Kingsmill, Y. Serra, and S. E. Yuter, 2000: Convection over the Pacific warm pool in relation to the atmospheric Kelvin–Rossby wave. *J. Atmos. Sci.,* **57,** 3058–3089.

Huffman, G. J., R. F. Adler, M. Morrissey, D. T. Bolvin, S. Curtis, R. Joyce, B. McGavock, and J. Susskind, 2001: Global precipitation at one-degree daily resolution from multisatellite observations. *J. Hydrometeor.,* **2,** 36–50.

Jakob, C., and G. Tselioudis, 2003: Objective identification of cloud regimes in the tropical western Pacific. *Geophys. Res. Lett.,* **30,** 2082, doi:10.1029/2003GL018367.

——, and C. Schumacher, 2008: Precipitation and latent heating characteristics of the major tropical western Pacific cloud regimes. *J. Climate,* **21,** 4348–4364.

Kalnay, E., and Coauthors, 1996: The NCEP/NCAR 40-Year Reanalysis Project. *Bull. Amer. Meteor. Soc.,* **77,** 437–471.

Kiladis, G. N., and K. M. Weickmann, 1992: Circulation anomalies associated with tropical convection during northern winter. *Mon. Wea. Rev.,* **120,** 1900–1923.

——, K. H. Straub, and P. T. Haertel, 2005: Zonal and vertical structure of the Madden–Julian oscillation. *J. Atmos. Sci.,* **62,** 2790–2809.

Knutson, T. R., and K. M. Weickmann, 1987: 30–60-day atmospheric oscillations: Composite life cycles of convection and circulation anomalies. *Mon. Wea. Rev.,* **115,** 1407–1436.

Lau, K.-M., and L. Peng, 1987: Origin of low-frequency (intraseasonal) oscillations in the tropical atmosphere. Part I: Basic theory. *J. Atmos. Sci.,* **44,** 950–972.

Lin, X., and R. H. Johnson, 1996: Kinematic and thermodynamic characteristics of the flow over the western Pacific warm pool during TOGA COARE. *J. Atmos. Sci.,* **53,** 695–715.

Luo, Z., and W. B. Rossow, 2004: Characterizing tropical cirrus life cycle, evolution, and interaction with upper-tropospheric water vapor using Lagrangian trajectory analysis of satellite observations. *J. Climate,* **17,** 4541–4563.

Madden, R. A., and P. R. Julian, 1994: Observations of the 40–50-day tropical oscillation—A review. *Mon. Wea. Rev.,* **122,** 814–837.

Majda, A. J., S. N. Stechmann, and B. Khouider, 2007: Madden–Julian oscillation analog and intraseasonal variability in a multicloud model above the equator. *Proc. Natl. Acad. Sci. USA,* **104,** 9919–9924.

Maloney, E. D., and D. L. Hartmann, 1998: Frictional moisture convergence in a composite life cycle of the Madden–Julian oscillation. *J. Climate,* **11,** 2387–2403.

Mapes, B. E., S. Tulich, J. Lin, and P. Zuidema, 2006: The mesoscale convection life cycle: Building block or prototype for large-scale tropical waves? *Dyn. Atmos. Oceans,* **42,** 3–29, doi:10.1016/j.dynatmoce.2006.03.003.

Matthews, A. J., 2000: Propagation mechanisms for the Madden–Julian oscillation. *Quart. J. Roy. Meteor. Soc.,* **126,** 2637–2651.

Milliff, R. F., and R. A. Madden, 1996: The existence and vertical structure of fast, eastward-moving disturbances in the equatorial troposphere. *J. Atmos. Sci.,* **53,** 586–597.

Moncrieff, M. W., 2004: Analytic representation of the large-scale organization of tropical convection. *J. Atmos. Sci.,* **61,** 1521–1538.

Mu, M., and G. J. Zhang, 2008: Energetics of Madden Julian oscillations in the NCAR CAM3: A composite view. *J. Geophys. Res.,* **113,** D05108, doi:10.1029/2007JD008700.

Myers, D. S., and D. E. Waliser, 2003: Three-dimensional water vapor and cloud variations associated with the Madden–Julian oscillation during Northern Hemisphere winter. *J. Climate,* **16,** 929–950.

Neelin, J. D., I. M. Held, and K. H. Cook, 1987: Evaporation–wind feedback and low-frequency variability in the tropical atmosphere. *J. Atmos. Sci.,* **44,** 2341–2348.

Pohl, B., and A. J. Matthews, 2007: Observed changes in the lifetime and amplitude of the Madden–Julian oscillation associated with interannual ENSO sea surface temperature anomalies. *J. Climate,* **20,** 2659–2674.

Raymond, D. J., 2001: A new model of the Madden–Julian oscillation. *J. Atmos. Sci.,* **58,** 2807–2819.

Rossow, W. B., and R. A. Schiffer, 1999: Advances in understanding clouds form ISCCP. *Bull. Amer. Meteor. Soc.,* **80,** 2261–2287.

——, and C. Pearl, 2007: 22-year survey of tropical convection penetrating into the lower stratosphere. *Geophys. Res. Lett.,* **34,** L04803, doi:10.1029/2006GL028635.

——, G. Tselioudis, A. Polak, and C. Jakob, 2005: Tropical climate described as a distribution of weather states indicated by distinct mesoscale cloud property mixtures. *Geophys. Res. Lett.,* **32,** L21812, doi:10.1029/2005GL024584.

Salby, M. L., R. R. Garcia, and H. H. Hendon, 1994: Planetary-scale circulations in the presence of climatological and wave-induced heating. *J. Atmos. Sci.,* **51,** 2344–2367.

Slingo, J. M., and Coauthors, 1996: Intraseasonal oscillations in 15 atmospheric general circulation models: Results from an AMIP diagnostic subproject. *Climate Dyn.,* **12,** 325–357.

——, D. P. Rowell, K. R. Sperber, and F. Nortley, 1999: On the predictability of the interannual behaviour of the Madden–Julian oscillation and its relationship with El Niño. *Quart. J. Roy. Meteor. Soc.,* **125,** 583–609.

Stephens, G. L., P. J. Webster, R. H. Johnson, R. Engelen, and T. L'Ecuyer, 2004: Observational evidence for the mutual regulation of the tropical hydrological cycle and tropical sea surface temperature. *J. Climate,* **17,** 2213–2224.

Tian, B., D. E. Waliser, and E. Fetzer, 2006: Modulation of the diurnal cycle of tropical deep convective clouds by the MJO. *Geophys. Res. Lett.,* **33,** L20704, doi:10.1029/2006GL027752.

Tung, W.-W., and M. Yanai, 2002: Convective momentum transport observed during the TOGA COARE IOP. Part I: General features. *J. Atmos. Sci.,* **59,** 1857–1871.

Wang, B., and H. Rui, 1990: Dynamics of the coupled moist Kelvin–Rossby wave on an equatorial ß plane. *J. Atmos. Sci.,* **47,** 397–413.

——, and Y. Xue, 1992: Behavior of a moist Kelvin wave packet with nonlinear heating. *J. Atmos. Sci.,* **49,** 549–559.

Wheeler, M. C., and H. H. Hendon, 2004: An all-season real-time multivariate MJO index: Development of an index for monitoring and prediction. *Mon. Wea. Rev.,* **132,** 1917–1932.

——, G. N. Kiladis, and P. J. Webster, 2000: Large-scale dynamical fields associated with convectively coupled equatorial waves. *J. Atmos. Sci.,* **57,** 613–640.

Woolnough, S. J., and J. M. Slingo, 2000: The relationship between convection and sea surface temperature on intraseasonal timescales. *J. Climate,* **13,** 2086–2104.

Yang, G.-Y., B. Hoskins, and J. Slingo, 2003: Convectively coupled equatorial waves: A new methodology for identifying wave structures in observational data. *J. Atmos. Sci.,* **60,** 1637–1654.

Zhang, C., 1996: Atmospheric intraseasonal variability at the surface in the western Pacific Ocean. *J. Atmos. Sci.,* **53,** 739–785.

——, 2005: Madden-Julian Oscillation. *Rev. Geophys.,* **43,** RG2003, doi:10.1029/2004RG000158.

Zhang, Y., W. B. Rossow, A. A. Lacis, V. Oinas, and M. I. Mishchenko, 2004: Calculation of radiative fluxes from the surface to top of atmosphere based on ISCCP and other global data sets: Refinements of the radiative transfer model and the input data. *J. Geophys. Res.,* **109,** D19105, doi:10.1029/2003JD004457.